

Article

Industrial Wastewater Discharge Retrieval Based on Stable Nighttime Light Imagery in China from 1992 to 2010

Zhaofu Li ^{1,*}, Hongyu Liu ², Chuan Luo ¹, Panpan Li ¹, Hengpeng Li ³ and Zhengqin Xiong ¹

¹ College of Resources and Environmental Science, Nanjing Agricultural University, Nanjing 210095, China; E-Mails: lc_notek@163.com (C.L.); lpp2012103100@126.com (P.L.); zqxiong@njau.edu.cn (Z.X.)

² College of Geography, Nanjing Normal University, Nanjing 210023, China; E-Mail: 09187@njnu.edu.cn

³ Nanjing Institute of Geography & Limnology, Chinese Academy of Science, Nanjing 210008, China; E-Mail: hpli@niglas.ac.cn

* Author to whom correspondence should be addressed; E-Mail: lizhaofu@njau.edu.cn; Tel.: +86-25-8439-5430; Fax: +86-25-8439-5210.

Received: 14 May 2014; in revised form: 8 August 2014 / Accepted: 11 August 2014 /

Published: 14 August 2014

Abstract: Industrial wastewater (IW) discharge, which is a known point source of pollution, is a major water pollution source. Increasing IW discharge has imposed considerable pressure on regional or global water environments. It is important to estimate the IW distribution in grid units to improve basin-scale hydrological processes and water quality modeling. For the first time, we use the nighttime light imagery produced by the Defense Meteorological Satellite Program's Operational Linescan System (DMSP/OLS) to estimate the spatial and temporal variations in the IW distribution from 1992 to 2010 in China. The digital number values per unit area (DNP) of each stable light image were calculated using nighttime light imagery and were regressed against the IW per unit area (IWP) to estimate the total industrial wastewater (TIW) for each province. The results indicated strong positive correlations between the DNP and the IWP for each province during different years. The fitted linear regression models were used to estimate IW discharge in China with reliable accuracy. The IW estimation using the satellite data was consistent with the statistical results. The results also revealed that the IW discharge coverage expanded, whereas the IW discharge intensity decreased from 1992 to 2010 in China.

Keywords: industrial wastewater; retrieval; DMSP/OLS; nighttime light imagery; digital number (DN); gross industrial production (GIP); China

1. Introduction

Economic development and population growth have caused depletion of global water resources and serious problems for water environments [1–3]. A key challenge to sustaining future water environments is estimating both current and future water pollution. Population growth and increasing food requirements have caused increasingly serious domestic sewage and agricultural diffuse source pollution [4]. Moreover, rapid economic development, especially in industrial enterprises, creates more industrial wastewater [5]. With increasing point and non-point source pollution, the threat to the global water environment has become more severe [6]. Water environmental problems are particularly challenging in China, because China has the largest population, a fast-growing economy, a rising water demand, relatively scarce water resources, a dated infrastructure and inadequate governance [7]. Understanding the spatial characteristics and differences in wastewater discharge is important for the development of a water conservancy plan in China.

Industrial wastewater (IW) has been the most important source of water pollution since the Industrial Revolution [8]. A country's IW is the total volume from each province, which is typically determined by adding the wastewater discharge from each administrative region. Currently, IW data are obtained from official statistical data that are collected by different administrative divisions, *i.e.*, the province, county, township, the prefecture under the provinces and the village under the townships. However, water environmental problems generally occur at the basin or watershed scales, which correspond to the best natural unit for performing water pollution research and management [9,10]. Because hydrological processes and the establishment of water quality occur within individual basins, a distributed model that is based on a raster grid or hydrological response units (HRUs) is the most efficient method for examining problems related to water environments [11,12]. IW statistical data that are based on an administrative unit cannot be applied to hydrological processes or be used in a water quality model on the basin scale. Therefore, the use of basin-scale statistical IW data is an important issue.

Considering that population, gross domestic product (GDP) or other socio-economic factors can be spatialized to grid cells retrieved from remote sensing data [13,14], we intended to establish a relationship between the IW statistical data and the remote sensing data. The Operational Linescan System (OLS) is a sensor controlled by the Defense Meteorological Satellite Program (DMSP). This instrument can detect nocturnal artificial lighting under clear night sky conditions without moonlight due to its low-light imaging capability [15]. The nighttime light (NTL) data collected by the DMSP/OLS measure the light on the Earth's surface, such as that generated by human settlements, gas flares, fires and illuminated marine vessels [16]. Previous studies have shown that the DMSP/OLS nighttime light imagery is a reliable tool for monitoring the spatial distribution of human settlements and for evaluating socioeconomic parameters [17–20]. Moreover, several studies have shown a strong relationship between the NTL data and important socioeconomic variables, such as urbanization

dynamics [16,21–24], urban population estimates [25,26], population density [27,28], economic activity [29], GDP [14,30], energy consumption [20,31–33] and the distribution of released anthropogenic heat [34]. Recently, progress has been achieved in environmental issues, such as CO₂ emissions [33], the global distribution of anthropogenic nitrogen oxide emissions [35] and the global water footprint [3], using DMSP/OLS nighttime light imagery. However, no study has applied the NTL data to examine industrial wastewater, the chemical oxygen demand (COD) or discharged ammonia nitrogen (NH₃N) at national or global scales.

The primary objective of this study was to evaluate whether DMSP/OLS NTL data can be used as a potential remote sensing data source for estimating IW, COD and NH₃N discharge spatial distributions in China. Statistical relationships between the NTL data digital number (DN) values and the industrial wastewater parameters were first determined for all provinces in China. Then, we interpreted the differences between the estimated IW discharge determined from the nighttime light imagery and the official statistical data. Finally, we analyzed the spatial and temporal variations in the industrial wastewater discharge from 1992 to 2010 in China.

2. Data and Methods

Nearly twenty years of DMSP/OLS stable light data (from 1992 to 2010) were used in this study. The data were obtained from version 4 of the NTL data and downloaded from the website of the National Geophysical Data Center (NGDC) at the National Oceanic and Atmospheric Administration (NOAA) [36]. The version 4 data contain 3000-km swath width NTL scan lines that are divided into an array of grids with a 0.55-km spatial resolution, which are aggregated and composited into 30 arc second grids. Each grid in the composite data contains a digital number (DN) that indicates the average nighttime light intensity observed within each year. Because the OLS passes over each location every day, multiple observations may be available for any single location over the course of a year. Several constraints were considered to identify the best quality nighttime light data for producing the composite image [37]. For example, ephemeral events, such as wildfires, were discarded. The final dataset contained lights from urban areas and other sites with persistent lighting, including gas flares. Background noise in the composite image was identified and replaced with a value of zero; the final DN values ranged from 0 to 63 [16]. Previous studies have shown that there was no substantial difference among the various satellite datasets in different years [34]. Therefore, it is feasible for the data from different nighttime light detection satellites to be applied in this study.

A series of datasets were utilized to analyze the relationship between the light DN values and the IW discharge in China. The amount of discharged industrial wastewater and the gross industrial production (GIP) data for each province from 1992 to 2010 were obtained from the China Statistical Yearbooks from 1993 to 2011 [38]. These yearbooks were compiled by the National Bureau of Statistics of China and contain detailed statistics on all societal aspects in China, including the economy, population and resources. The statistics were separately compiled for each province and district.

To obtain the correct area for analyzing the statistical relationship between the NTL and IW datasets, the ordinary spatial reference of the geographic coordinate system that was related to the WGS 84 datum was transformed to the Albers equal-area projection in China. Moreover, the spatial resolution of the NTL data was resampled to a 1 km × 1 km area. Vector data for the Chinese

provincial boundaries were also transformed to an equal-area projection. The provincial boundary map was overlaid on the nighttime light images, and the DN values per unit area (DNP) for all provinces were calculated for each of the 19 years from 1992 to 2010. The total IW (TIW) discharge for each province divided by the area of the province represents the amount of discharged IW per unit area (IWP). Then, statistical relationships between the IWP and the DNP were analyzed. The relative difference (RD) between the predicted TIW (PTIW) and the statistical TIW (STIW) was calculated as follows to analyze the accuracy of the fitted models:

$$RD = (PTIW - STIW)/STIW \quad (1)$$

where PTIW is the predicted total IW from the nighttime light image and STIW is the statistical total IW. For the COD and NH₃N discharge calculation and analysis, similar methods were adopted. The acronyms of the variables involved in the calculations and analyses are shown in Table 1.

Table 1. Acronyms of the variables involved in the calculations and analyses. COD, chemical oxygen demand; NTL, nighttime light.

Acronym	TIW	PTIW	STIW	IWP	DNP	TDN
Full Name	Total industrial water discharge	Predicted TIW from nighttime light image	Statistical TIW by National Bureau of Statistics of China	Industrial wastewater discharge per unit area	Digital number per unit area	Total nighttime light digital number values
Acronym	GIP	IWCOD	IWNH3N	IWCODP	IWNH3NP	
Full Name	Gross Industrial Production	Quantity of COD in industrial wastewater	Quantity of ammonia nitrogen in industrial wastewater	COD discharge amount per unit area or unit NTL light values	Ammonia nitrogen discharge amount per unit area	

3. Results and Discussion

3.1. Relationship and Fitted Model between the DMSP/OLS Data and the Industrial Wastewater Discharge

The industrial wastewater discharge per unit area (IWP) from 1992 to 2010 was calculated by dividing the TIW by the area of each province in China. The NTL digital number values per unit area (DNP) for all of the provinces were calculated using the ArcGIS zonal statistics tool. The relationship between the IWP and the DNP for each year was analyzed. Moreover, a linear model was fitted to the data and used to estimate the industrial wastewater discharge from the NTL light imagery data.

The primary model criterion is that when the digital number (DN) of the nighttime image increases, the discharged IW should also increase. Therefore, the IW discharge was expected to increase with an increasing DN. Based on this assumption, different regression models, including the exponential, power function and quadratic polynomial models, were used. In addition, a statistical hypothesis test was conducted. A comparison among the different model results suggested that the linear model, *i.e.*, $y = kx + b$, performed the best. Here, k is the slope and b is the intercept of the linear function.

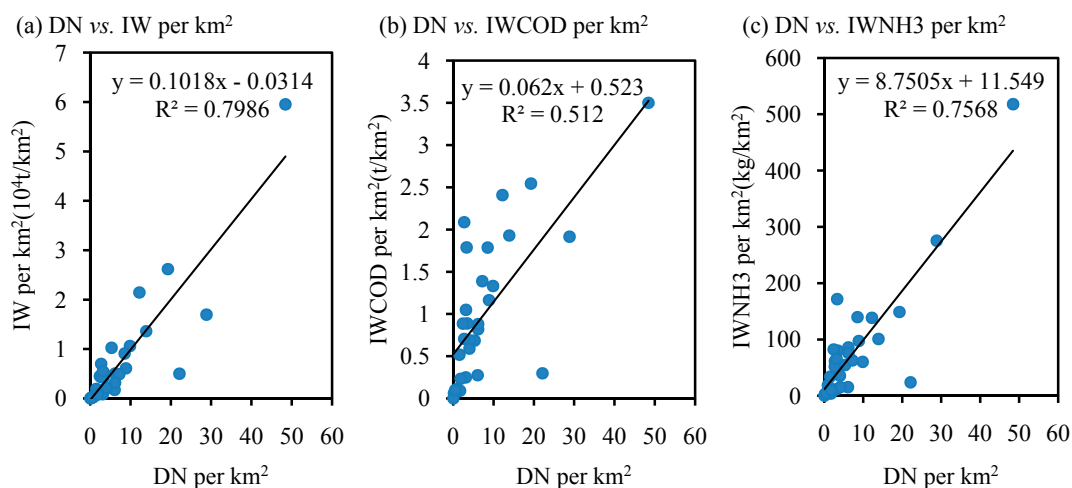
Figure 1a–c depicts the linear relationships between the DNP and the IWP, the IWCODP and the IWNH3NP for 31 provinces in 2010, respectively. A high correlation was observed between the DNP and the IWP (Figure 1a) and between the DNP and the IWNH3NP (Figure 1c); the corresponding R^2

values were 0.798 and 0.756, respectively. Although the correlation between the DNP and the IWCODP was the weakest among the three relationships (Figure 1b) with an R^2 value of 0.512, all of the correlations were significant at the 0.01 level. These results of quantitative analysis between DNP and IWP are consistent with the current situation in China, because industry is mainly distributed in urban regions with higher NTL DN values.

Furthermore, the model coefficients and the fitted model parameters for the relationships between the DNP and the IWP, IWCODP and IWNH3NP for all the provinces were calculated for each year. Table 2 shows the Pearson correlation coefficient (r), the slope (k) and the determination coefficient of the linear regression models that were constructed between the DNP and the IWP, IWCODP and IWNH3NP for 31 provinces from 1992 to 2010.

Significant positive correlations between the DNP and the IWP, IWCODP and IWNH3NP are shown in Table 2. All of the Pearson correlation coefficients for the relationship between the DNP and the IWP exceeded 0.85, while the correlation coefficients range from 0.716 to 0.849 for the relationship between the DNP and the IWCODP in different years. Although the correlation coefficients between the DNP and the IWNH3NP were relatively low, *i.e.*, ranging from 0.627 to 0.870, all of the values exhibited a significant correlation at the 0.01 level according to a two-tailed test. Generally, the linear relationships between the DNP and the IWP, the IWCODP and the IWNH3NP were significant in each year.

Figure 1. (a) The relationship between the DNP and the IWP (for 31 provinces); (b) the relationship between the DNP and the IWCODP (for 31 provinces); (c) the relationship between the DNP and the IWNH3NP (for 31 provinces) in 2010.



Based on the previous assumption and the analyses between the DNP and the IW discharge variables, the slope and determination coefficients of the linear regression functions were obtained for each year (Table 2). These parameters and functions can be used to estimate the IW spatial distribution from the NTL light data in China.

Table 2. The Pearson correlation coefficient (r), linear regression model slope (k) and determination coefficient (R^2) between the DNP and the IWP (unit: 10^4 t/km²), the IWCODP (unit: t/km²) and the IWNH3NP (unit: kg/km²) for 31 provinces from 1992 to 2010.

Year	r between the DNP and the IWP	k of the IWP Regression Model	R^2 of the IWP Regression Model	r between the DNP and the IWCODP	k of the IWCODP Regression Model	R^2 of the IWCODP Regression Model	r between the DNP and the IWNH3NP	k of the IWNH3NP Regression Model	R^2 of the IWNH3NP Regression Model
1992	0.865**	0.807	0.747	-	-	-	-	-	-
1993	0.856**	0.732	0.732	-	-	-	-	-	-
1994	0.883**	0.529	0.779	-	-	-	-	-	-
1995	0.873**	0.510	0.762	-	-	-	-	-	-
1996	0.852**	0.535	0.726	-	-	-	-	-	-
1997	0.866**	0.415	0.750	-	-	-	-	-	-
1998	0.869**	0.380	0.754	-	-	-	-	-	-
1999	0.868**	0.354	0.753	-	-	-	-	-	-
2000	0.887**	0.297	0.786	-	-	-	-	-	-
2001	0.879**	0.277	0.772	-	-	-	-	-	-
2002	0.891**	0.242	0.793	-	-	-	-	-	-
2003	0.914**	0.260	0.835	0.849**	0.195	0.721	0.774**	15.99	0.599
2004	0.914**	0.217	0.835	0.819**	0.153	0.670	0.675**	11.10	0.455
2005	0.926**	0.199	0.857	0.793**	0.157	0.629	0.627**	11.76	0.393
2006	0.913**	0.180	0.833	0.790**	0.134	0.623	0.772**	11.98	0.595
2007	0.909**	0.177	0.826	0.789**	0.126	0.622	0.815**	11.45	0.664
2008	0.908**	0.158	0.819	0.763**	0.103	0.565	0.835**	9.981	0.679
2009	0.873**	0.142	0.761	0.753**	0.098	0.567	0.809**	7.693	0.654
2010	0.894**	0.101	0.798	0.716**	0.062	0.512	0.870**	8.750	0.756

** Represents that the correlation is significant at the 0.01 level (two-tailed); “-” indicates no data; $n = 31$.

3.2. Differences between the TIW Predicted from the Nighttime Lights Data and the Statistical TIW

The IWP was estimated using the linear regression model (as Table 2 shown) for each grid in China. The total IW (TIW) for each province was calculated as the total of the values from all of the grids within each province using the ArcGIS zonal statistics tool. Then, the predicted TIW (PTIW) was compared with the official statistical TIW (STIW) for all of the provinces.

Table 3 shows the differences between the PTIW estimated from the nighttime lights data and the STIW for 31 provinces in 2010. As shown in Table 3, the linear model results were reasonable in most provinces, whereas significant errors occurred in specific areas. The relative difference ranged from 0 to 0.5 in 16 of the 31 provinces, whereas the model exhibited significant errors in five provinces (*i.e.*, the difference rate exceeded one). Despite these errors, the DMSP/OLS data provided useful estimates of the IW, IWCOD and IWNH3N spatial distributions in China, exhibiting a total error of -8.2% . Theoretically, industrial wastewater discharge is closely correlated with industrial development and the DMSP/OLS NTL data. The large relative difference may primarily be related to the significant differences in economic development in different areas.

Previous studies have shown that the DMSP/OLS data are closely correlated with the social and economic activities, such as the GDP and the population distribution [14,19]. For regions in which economic development was accompanied by industrial wastewater discharge, Table 3 demonstrates that the linear regression model results are generally credible. However, for regions in which economic development did not significantly rely on industrial activities, a significant estimation error occurred in the model. For example, the estimates were more accurate for the provinces with a higher percentage of STIW in China, such as Shandong, Henan, Guangdong and Jiangsu. The areas in which the model results overestimated the actual statistical data were typically the provinces that exhibited primary and tertiary industrial growth; these activities are typically related to less industrial wastewater being discharged in the process of economic development. These areas included Xizang, Beijing, Hainan, Qinghai, Heilongjiang, Yunnan and Jilin. Although the IW discharge was overestimated, the percentages of the TIW in China are very low in these provinces. Moreover, the error was not obvious in the national IW discharge amount. The model underestimated the results for the developing areas in which industry is important and the production efficiency is relatively low, such as in Guangxi, Hunan and Fujian provinces. In these regions, the IW discharge per unit gross industrial production (GIP) was higher.

Consequently, regional differences in industrial productivity for economic development may be a major reason for the model errors. Industrial wastewater discharge is closely correlated with industry development and the DN values obtained from the DMSP/OLS NTL data. However, the relationship between the industrial wastewater discharge efficiency and the NTL DN value is complex.

Table 3. Difference rate between the PTIW and the STIW for 31 provinces in China in 2010.

Regions	The PTIW from Nighttime Light Images (10^4 t/year)	STIW (10^4 t/year)	Difference Rate	Percentage of the STIW in China (%)	Gross Industrial Production (GIP) (10^8 ¥)	The STIW per 10^8 Yuan of GIP (10^4 t/ 10^8 ¥)
Jiangsu	193,209	263,760	-0.27	11.1	21,753.93	12.12
Zhejiang	122,004	217,426	-0.44	9.2	14,297.93	15.21
Shandong	209,951	208,257	0.01	8.8	21,238.49	9.81
Guangdong	169,951	187,031	-0.09	7.9	23,014.53	8.13
Guangxi	57,405	165,211	-0.65	7.0	4511.68	36.62
Henan	137,566	150,406	-0.09	6.3	13,226.38	11.37
Fujian	61,161	124,168	-0.51	5.2	7522.83	16.51
Hebei	161,895	114,232	0.42	4.8	10,707.68	10.67
Hunan	45,013	95,605	-0.53	4.0	7343.19	13.02
Hubei	59,487	94,593	-0.37	4.0	7767.24	12.18
Sichuan	59,207	93,444	-0.37	3.9	8672.18	10.78
Jiangxi	40,408	72,526	-0.44	3.1	5122.88	14.16
Liaoning	101,177	71,521	0.41	3.0	9976.82	7.17
Anhui	83,145	70,971	0.17	3.0	6436.62	11.03
Shanxi	92,877	49,881	0.86	2.1	5234.00	9.53
Shaanxi	77,147	45,487	0.70	1.9	5446.10	8.35
Chongqing	23,668	45,180	-0.48	1.9	4359.12	10.36

Table 3. Cont.

Regions	The PTIW from Nighttime Light Images (10^4 t/year)	STIW (10^4 t/year)	Difference Rate	Percentage of the STIW in China (%)	Gross industrial Production (GIP) (10^8 ¥)	The STIW per 10^8 Yuan of GIP (10^4 t/ 10^8 ¥)
Inner Mongolia	51,152	39,536	0.29	1.7	6367.69	6.21
Heilongjiang	128,012	38,921	2.29	1.6	5204.11	7.48
Jilin	73,122	38,656	0.89	1.6	4506.31	8.58
Shanghai	29,966	36,696	-0.18	1.5	7218.32	5.08
Yunnan	59,218	30,926	0.91	1.3	3223.49	9.59
Xinjiang	30,440	25,413	0.20	1.1	2592.15	9.80
Ningxia	15,764	21,977	-0.28	0.9	827.91	26.55
Tianjin	33,444	19,680	0.70	0.8	4840.23	4.07
Gansu	24,666	15,352	0.61	0.6	1984.97	7.73
Guizhou	24,711	14,130	0.75	0.6	1800.06	7.85
Qinghai	-9,616	9031	-2.06	0.4	744.63	12.13
Beijing	36,141	8198	3.41	0.3	3388.38	2.42
Hainan	19,494	5782	2.37	0.2	571.00	10.13
Xizang	-32,445	736	-45.08	0.0	163.92	4.49
China	2,179,338	2,374,733	-0.082	100.0	220,064.77	10.79

3.3. Spatial and Temporal Variations in the Chinese IW Discharge Distribution

The spatial distribution of the grid-scale IW discharge from 1992 to 2010 in China is shown in Figure 2. The annual evolution of the IW discharge was comparable to economic development and urban expansion in China.

The IW discharge was spatially concentrated in eastern, northeastern and southeastern China, especially in the Jing-Jin-Ji urban circle, the Yangtze River Delta, the Pearl River Delta and other coastal cities of China. The results show that the inland cities appear as spots on the IW distribution map, whereas the eastern portion of China and the coastal cities exhibit an intermittent distribution pattern (Figure 2).

The increasing IW discharge area and decreasing IW discharge intensity (IW discharge quantity per km^2) trends are clearly depicted in Figure 2. The IW distribution in 1992 (Figure 2a) suggests that the IW discharge area was not extensive, except in economically developed areas, in which the discharge intensity was high. Several years later, the IW discharge region expanded beyond the developed areas. A significant enhancement in the IW discharge in eastern China is shown in the IW discharge distribution map in 1998 (Figure 2b). The trend in the IW distribution in 2004 (Figure 2c) and 2010 (Figure 2d) in China suggests that the IW discharge region continued to expand. For the IWCOD and the IWNH₃N distributions, the spatial patterns and the temporal trends were consistent with the IW distribution. The extent of the distribution clearly broadened from 2003 (Figure 2e,g) to 2010 (Figure 2f,h).

The temporal changes in the IW discharge intensity exhibit a good trend. Figure 2 shows that the trend in the IW distribution in China suggests that the IW discharge intensity gradually decreased,

although the IW discharge region continued to expand. This trend is also shown in Table 2 in which the slope of the linear regression model decreases from 1992 to 2010. A decreasing slope indicates that the IW discharge intensity decreased even though the light DN values remained constant each year. The highest predicted IW discharge intensity decreased from $50.071 \times 10^4 \text{ t}\cdot\text{km}^{-2}$ in 1992 to $6.332 \times 10^4 \text{ t}\cdot\text{km}^{-2}$ in 2010. The highest IWCOD discharge intensity decreased from $12.815 \text{ t}\cdot\text{km}^{-2}$ in 2003 to $4.429 \text{ t}\cdot\text{km}^{-2}$ in 2010. Moreover, the highest IWNH₃N discharge intensity also decreased from $1057.05 \text{ kg}\cdot\text{km}^{-2}$ in 2003 to $562.79 \text{ kg}\cdot\text{km}^{-2}$ in 2010. According to these findings, the total IW discharge increased in conjunction with economic growth. However, the IW discharge intensity decreased due to economic development.

Figure 2. Estimated industrial wastewater discharge distribution in China. (a–d) The predicted IWP ($10^4 \text{ t}\cdot\text{km}^{-2}$) distribution in 1992, 1998, 2004 and 2010, respectively; (e–f) the predicted IWCODP ($\text{t}\cdot\text{km}^{-2}$) distribution in 2003 and 2010, respectively; and (g–h) the predicted IWNH₃NP (kg/km^2) distribution in 2003 and 2010, respectively.

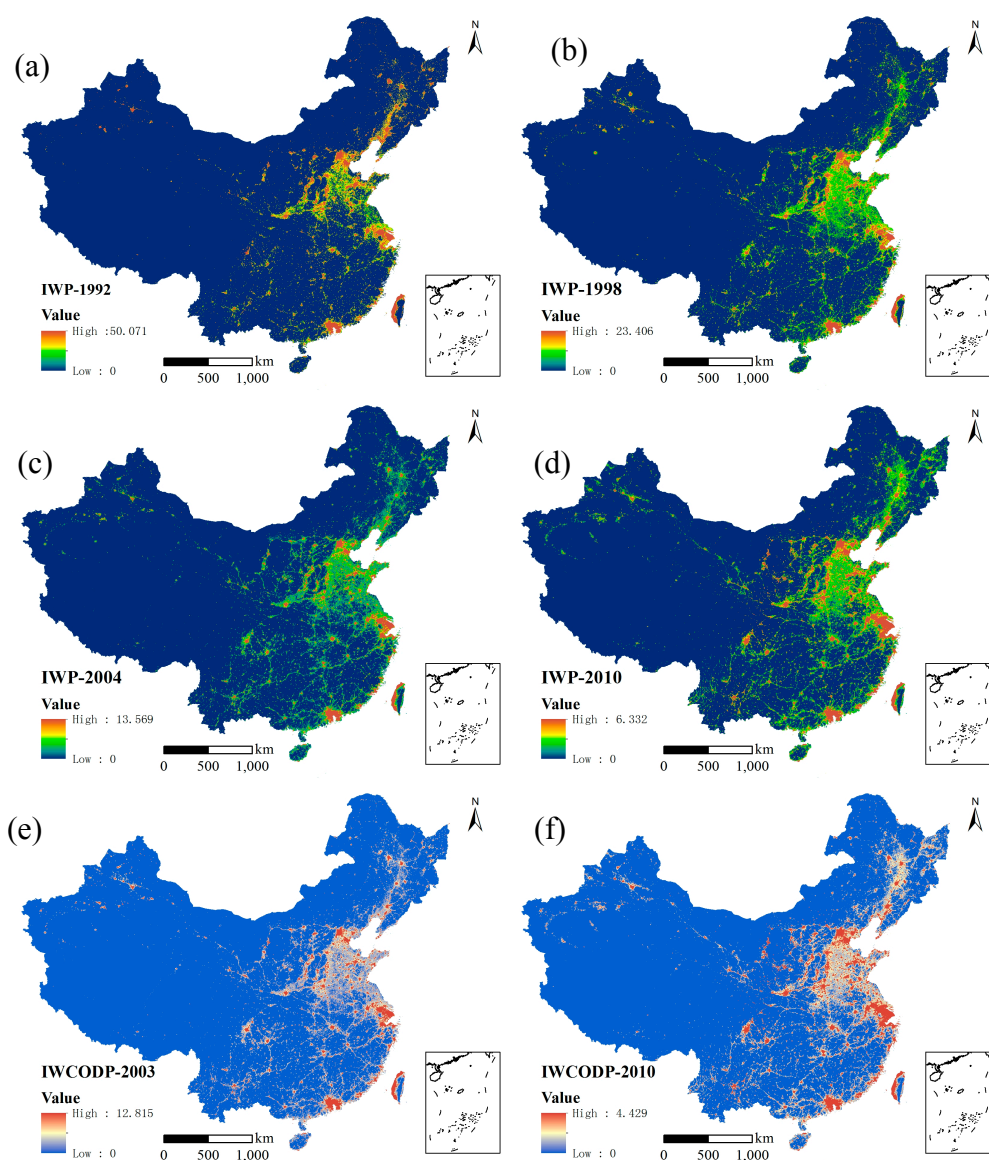


Figure 2. Cont.

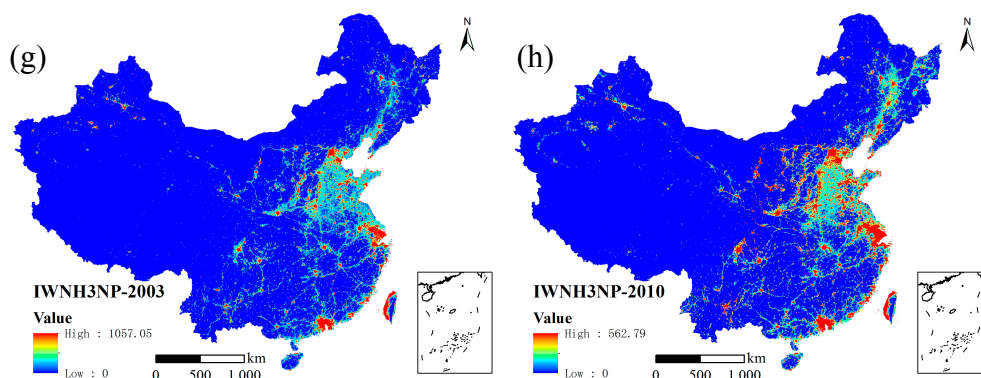
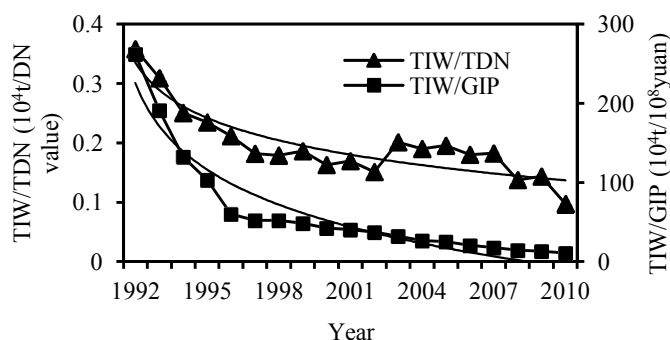


Figure 3 shows the ratio of the TIW to the total DN (TDN) and the TIW to the GIP from 1992 to 2010 in China. An obvious decreasing trend was observed. The IW discharge quantity per light DN value decreased gradually over the 20-year period. The trend was similar to the variations in the GIP to the TIW ratio. Similarly, the IW discharge per unit GIP decreased in conjunction with increased production efficiency in China.

Figure 3. Temporal trends in the TIW to the TDN ratio and the TIW to the GIP ratio from 1992 to 2010 in China.



4. Conclusions

This study highlighted the possibility of using the Defense Meteorological Satellite Program's Operational Linescan System (DMSP/OLS) nighttime light (NTL) imagery to retrieve both spatial and temporal variations in the industrial wastewater (IW) distribution from 1992 to 2010 in China. We found strong positive correlations between the digital number values per unit area (DNP) and the IW per unit area (IWP) for each province in different years. The Pearson correlation coefficients (r) between the DNP and the IWP are greater than 0.85, while the r ranges from 0.716 to 0.849 for the relationship between DNP and the chemical oxygen demand discharge amount per unit area (IWCODP). Moreover, the r between DNP and the ammonia nitrogen discharge amount per unit area (IWNH3NP) ranges from 0.627 to 0.870, and all of the values show a significant correlation at the 0.01 level.

Based on the fitted linear model between DNP and IWP, the DMSP/OLS NTL data provided a dependable estimation of the IW discharge with a total error of -8.2% in 2010. The estimation was

more accurate for the provinces with a higher percentage of IW discharge in China, such as Shandong, Henan, Guangdong, Jiangsu, *etc.* Fitted linear regression models could be used to estimate the IWP, the IWCODP and the IWNH3NP from 1992 to 2010 in China with reliable accuracy. The amount of IW estimated using the satellite data was consistent with the statistical results.

The industrial wastewater discharge distribution maps for individual grid units, which were produced using the satellite data, were significantly more credible and detailed compared to the statistical maps. The IW discharge was spatially concentrated in eastern, northeastern and southeastern China, especially in the Jing-Jin-Ji urban circle, the Yangtze River Delta, the Pearl River Delta and other coastal developed cities, while the IW discharge is lower in undeveloped areas, such as northwestern and southwestern provinces in China. The grid-scale industrial wastewater discharge data retrieved from the NTL data can be used in large-scale basin water quality models. The results also revealed that the IW discharge coverage expanded while the IW discharge intensity decreased from 1992 to 2010 in China. The maximum of IWP changed from $50.071 \times 10^4 \text{ t}\cdot\text{km}^{-2}$ in 1992 to $6.332 \times 10^4 \text{ t}\cdot\text{km}^{-2}$ in 2010. The maximum of IWCODP decreased from $12.815 \text{ t}\cdot\text{km}^{-2}$ in 2003 to $4.429 \text{ t}\cdot\text{km}^{-2}$ in 2010, and the maximum of IWNH3NP also decreased from $1,057.05 \text{ kg}\cdot\text{km}^{-2}$ in 2003 to $562.79 \text{ kg}\cdot\text{km}^{-2}$ in 2010.

Future endeavors should improve the prediction accuracy by considering other factors that affect the IW discharge in the fitted regression models. The use of satellite imagery by integrating industrial wastewater data, domestic sewage and agricultural non-point source pollution is another challenge for water environment pollution.

Acknowledgments

We sincerely appreciate the editor and the five anonymous reviewers for their critical and valuable comments to help improve this manuscript. This study was jointly supported by the National Natural Science Foundation of China (No. 41171071), the Priority Academic Program Development of Jiangsu Higher Education Institutions (PAPD), the Key Project of Chinese Academy of Sciences (KZZD-EW-10-4) and the Scientific Research Foundation for the Returned Overseas Chinese Scholars, State Education Ministry. Special thanks are extended to the Earth Observation Group, National Geophysical Data Center, and National Oceanic and Atmospheric Administration of the United States for providing the nighttime light imagery.

Author Contributions

Zhaofu Li and Hongyu Liu designed and performed the data analysis and authored the manuscript. Zhengqin Xiong and Hengpeng Li revised the manuscript and provided several important suggestions. Chuan Luo and Panpan Li collected the statistical data. All of the authors participated in editing and revising the paper.

Conflicts of Interest

The authors declare no conflict of interest.

References

1. Vörösmarty, C.J.; Green, P.; Salisbury, J.; Lammers, R.B. Global water resources: Vulnerability from climate change and population growth. *Science* **2000**, *289*, doi:10.1126/science.289.5477.284.
2. Rockström, J.; Lannerstad, M.; Falkenmark, M. Assessing the water challenge of a new green revolution in developing countries. *Proc. Natl. Acad. Sci. USA* **2007**, *104*, 6253–6260.
3. Zhao, N.; Ghosh, T.; Currit, N.A.; Elvidge, C.D. Relationships between satellite observed lit area and water footprints. *Water Resour. Manag.* **2011**, *25*, 2241–2250.
4. Novotny, V. Diffuse pollution from agriculture—A worldwide outlook. *Water Sci. Technol.* **1999**, *39*, 1–13.
5. Liu, J.; Diamond, J. China's environment in a globalizing world. *Nature* **2005**, *435*, 1179–1186.
6. Loucks, D.P.; van Beek, E. *Water Resources Systems Planning and Management—Facts about Water*; UNESCO: Paris, France, 2005.
7. Liu, J.; Yang, W. Water sustainability for china and beyond. *Science* **2012**, *337*, 649–650.
8. Rogers, P.; Silva, R.; Bhatia, R. Water is an economic good: How to use prices to promote equity, efficiency, and sustainability. *Water Policy* **2002**, *4*, 1–17.
9. Mitsch, W.J.; Day, J.W.; Gilliam, J.W.; Groffman, P.M.; Hey, D.L.; Randall, G.W.; Wang, N. Reducing nitrogen loading to the gulf of mexico from the mississippi river basin: Strategies to counter a persistent ecological problem ecotechnology—The use of natural ecosystems to solve environmental problems—Should be a part of efforts to shrink the zone of hypoxia in the gulf of Mexico. *BioScience* **2001**, *51*, 373–388.
10. Withers, P.J.; Lord, E.I. Agricultural nutrient inputs to rivers and groundwaters in the UK: Policy, environmental management and research needs. *Sci. Total Environ.* **2002**, *282*, 9–24.
11. Krysanova, V.; Müller-Wohlfeil, D.-I.; Becker, A. Development and test of a spatially distributed hydrological/water quality model for mesoscale watersheds. *Ecol. Model.* **1998**, *106*, 261–289.
12. Di Luzio, M.; Srinivasan, R.; Arnold, J.G. A GIS-coupled hydrological model system for the watershed assessment of agricultural nonpoint and point sources of pollution. *Trans. GIS* **2004**, *8*, 113–136.
13. Imran, M.; Stein, A.; Zurita-Milla, R. Investigating rural poverty and marginality in Burkina Faso using remote sensing-based products. *Int. J. Appl. Earth Obs. Geoinf.* **2014**, *26*, 322–334.
14. Wu, J.; Wang, Z.; Li, W.; Peng, J. Exploring factors affecting the relationship between light consumption and gdp based on DMSP/OLS nighttime satellite imagery. *Remote Sens. Environ.* **2013**, *134*, 111–119.
15. Elvidge, C.D.; Baugh, K.E.; Hobson, V.R.; Kihn, E.A.; Kroehl, H.W.; Davis, E.R.; Cocero, D. Satellite inventory of human settlements using nocturnal radiation emissions: A contribution for the global toolchest. *Glob. Chang. Biol.* **1997**, *3*, 387–395.
16. Zhang, Q.; Seto, K.C. Mapping urbanization dynamics at regional and global scales using multi-temporal DMSP/OLS nighttime light data. *Remote Sens. Environ.* **2011**, *115*, 2320–2329.
17. Small, C.; Elvidge, C.D. Night on earth: Mapping decadal changes of anthropogenic night light in Asia. *Int. J. Appl. Earth Obs. Geoinf.* **2013**, *22*, 40–52.
18. Small, C.; Pozzi, F.; Elvidge, C.D. Spatial analysis of global urban extent from DMSP-OLS night lights. *Remote Sens. Environ.* **2005**, *96*, 277–291.

19. Elvidge, C.D.; Baugh, K.E.; Kihn, E.A.; Kroehl, H.W.; Davis, E.R.; Davis, C.W. Relation between satellite observed visible-near infrared emissions, population, economic activity and electric power consumption. *Int. J. Remote Sens.* **1997**, *18*, 1373–1379.
20. Shi, K.; Yu, B.; Huang, Y.; Hu, Y.; Yin, B.; Chen, Z.; Chen, L.; Wu, J. Evaluating the ability of NPP-VIIRS nighttime light data to estimate the gross domestic product and the electric power consumption of China at multiple scales: A comparison with DMSP-OLS data. *Remote Sens.* **2014**, *6*, 1705–1724.
21. Yu, B.; Shu, S.; Liu, H.; Song, W.; Wu, J.; Wang, L.; Chen, Z. Object-based spatial cluster analysis of urban landscape pattern using nighttime light satellite images: A case study of China. *Int. J. Geogr. Inf. Sci.* **2014**, *5*, 1–28.
22. Wei, Y.; Liu, H.; Song, W.; Yu, B.; Xiu, C. Normalization of time series DMSP-OLS nighttime light images for urban growth analysis with Pseudo invariant features. *Landsc. Urban Plan.* **2014**, *128*, 1–13.
23. Sutton, P.C. A scale-adjusted measure of “urban sprawl” using nighttime satellite imagery. *Remote Sens. Environ.* **2003**, *86*, 353–369.
24. Shi, K.; Huang, C.; Yu, B.; Yin, B.; Huang, Y.; Wu, J. Evaluation of NPP-VIIRS night-time light composite data for extracting built-up urban areas. *Remote Sens. Lett.* **2014**, *5*, 358–366.
25. Yang, X.; Yue, W.; Gao, D. Spatial improvement of human population distribution based on multi-sensor remote-sensing data: An input for exposure assessment. *Int. J. Remote Sens.* **2013**, *34*, 5569–5583.
26. Amaral, S.; Monteiro, A.M.V.; Camara, G.; Quintanilha, J.A. DMSP/OLS night-time light imagery for urban population estimates in the Brazilian Amazon. *Int. J. Remote Sens.* **2006**, *27*, 855–870.
27. Zhuo, L.; Ichinose, T.; Zheng, J.; Chen, J.; Shi, P.J.; Li, X. Modelling the population density of china at the pixel level based on DMSP/OLS non-radiance-calibrated night-time light images. *Int. J. Remote Sens.* **2009**, *30*, 1003–1018.
28. Sutton, P.C.; Elvidge, C.; Obremski, T. Building and evaluating models to estimate ambient population density. *Photogramm. Eng. Remote Sens.* **2003**, *69*, 545–553.
29. Elvidge, C.D.; Imhoff, M.L.; Baugh, K.E.; Hobson, V.R.; Nelson, I.; Safran, J.; Dietz, J.B.; Tuttle, B.T. Night-time lights of the world: 1994–1995. *ISPRS J. Photogramm. Remote Sens.* **2001**, *56*, 81–99.
30. Triantakoustantis, D.; Stathakis, D. Cokriging areal interpolation for estimating economic activity using night-time light satellite data. *Lect. Notes Comput. Sci.* **2014**, *8582*, 243–252.
31. Chand, T.R.K.; Badarinath, K.V.S.; Elvidge, C.D.; Tuttle, B.T. Spatial characterization of electrical power consumption patterns over india using temporal DMSP-OLS night-time satellite data. *Int. J. Remote Sens.* **2009**, *30*, 647–661.
32. Letu, H.; Hara, M.; Yagi, H.; Naoki, K.; Tana, G.; Nishio, F.; Shuhei, O. Estimating energy consumption from night-time DMPS/OLS imagery after correcting for saturation effects. *Int. J. Remote Sens.* **2010**, *31*, 4443–4458.
33. He, C.; Ma, Q.; Li, T.; Yang, Y.; Liu, Z. Spatiotemporal dynamics of electric power consumption in Chinese mainland from 1995 to 2008 modeled using DMSP/OLS stable nighttime lights data. *J. Geogr. Sci.* **2012**, *22*, 125–136.

34. Chen, B.; Shi, G.; Wang, B.; Zhao, J.; Tan, S. Estimation of the anthropogenic heat release distribution in China from 1992 to 2009. *Acta Meteorol. Sin.* **2012**, *26*, 507–515.
35. Toenges-Schuller, N.; Stein, O.; Rohrer, F.; Wahner, A.; Richter, A.; Burrows, J.P.; Beirle, S.; Wagner, T.; Platt, U.; Elvidge, C.D. Global distribution pattern of anthropogenic nitrogen oxide emissions: Correlation analysis of satellite measurements and model calculations. *J. Geophys. Res. Atmos.* **2006**, *111*, doi:10.1029/2005JD006068.
36. NOAA National Geophysical Data Center. Version 4 DMSP-OLS Nighttime Lights Time Series. Available online: <http://ngdc.noaa.gov/eog/dmsp/downloadV4composites.html>. (accessed on 17 March, 2014).
37. Elvidge, C.D.; Erwin, E.H.; Baugh, K.E.; Ziskin, D.; Tuttle, B.T.; Ghosh, T.; Sutton, P.C. Overview of DMSP nighttime lights and future possibilities. In Proceedings of 2009 Joint Urban Remote Sensing Event, Shanghai, China, 20–22 May 2009; pp. 1665–1669.
38. National Bureau of Statistics of China. *China Statistical Yearbook (1993–2011)*; China Statistical Press: Beijing, China. (In Chinese)

© 2014 by the authors; licensee MDPI, Basel, Switzerland. This article is an open access article distributed under the terms and conditions of the Creative Commons Attribution license (<http://creativecommons.org/licenses/by/3.0/>).